Hybrid Semiconducting Polymer Dot–Quantum Dot with Narrow-Band Emission, Near-Infrared Fluorescence, and High Brightness

Yang-Hsiang Chan, Fangmao Ye, Maria Elena Gallina, Xuanjun Zhang, Yuhui Jin, I-Che Wu, and Daniel T. Chiu*

Department of Chemistry, University of Washington, Seattle, Washington 98195, United States

Ⓢ *Supporting Information*

ABSTRACT: This communication describes a new class of semiconducting polymer nanoparticle–quantum dot hybrid with high brightness, narrow emission, near-IR fluorescence, and excellent cellular targeting capability. Using this approach, we circumvented the current difficulty with obtaining narrow-band-emitting and near-IR-fluorescing semiconducting polymer nanoparticles while combining the advantages of both semiconducting polymer nanoparticles and quantum dots. We further demonstrated the use of this new class of hybrid nanomaterial for effective and specific cellular and subcellular labeling without any noticeable nonspecific binding. This hybrid nanomaterial is anticipated to find use in a variety of in vitro and in vivo biological applications.

There has been considerable effort in the design of nanostructured materials with highly integrated functionalities because of their potential use in diverse applications, such as multimodality imaging, optoelectronics, and nanomedicine.[1−7] In particular, fluorescent inorganic nanoparticles (NPs), often called quantum dots (Qdots), have attracted much attention in the past decade because of their unique optical features, including high quantum yields, large effective Stokes shifts, and broad absorption with narrow emission in which the emission wavelength can be tuned by changing the size of the Qdots.[8−12]

Recently, semiconducting polymer NPs (Pdots) have emerged as a new class of highly fluorescent nanomaterials that exhibit extraordinary fluorescence brightness, excellent photostability, and high emission rates.[13−28] There is, however, a significant drawback to Pdots at present: most of the reported semiconducting polymers used to form Pdots have broad emission bands.[13,17] This drawback greatly limits the multiplexing capability of Pdots, because broadband emission can result in spectral interference with other fluorophores, especially for Pdots with high brightness, where leakage of emitted photons into other detection channels can easily overwhelm the fluorescence from other non-Pdot probes. Moreover, the synthesis of suitable near-IR (NIR)-fluorescing semiconducting polymers (700−1000 nm) for generating Pdots remains a difficult challenge, in part because of the self-quenching of NIR polymers upon condensation into a Pdot form.

A key aim in the design of hybrid nanomaterials is to enhance the beneficial signature properties of one component while preserving the desired characteristics of the other(s). To demonstrate this concept and to address the above-mentioned drawbacks of Pdots, this communication reports a facile, versatile, and scalable strategy that can integrate the optical properties of both Qdots and Pdots without sacrificing their functionalities. The high brightness of Pdots is derived in part from the large absorption cross section of the semiconducting polymer. The Pdot−Qdot hybrid integrates the high absorption cross section offered by Pdots and the narrow emission and NIR fluorescence available from Qdots. The approach is based on the replacement of the surfactants of CdSe Qdots by a poly[9,9-dioctylfluorenyl-2,7-diyl)-*co*-4,7-benzo{2,1,3}-thiadiazole)] (PFBT) polymer derivative followed by the co-nanoprecipitation of the functionalization polymers, semiconducting polymers, and CdSe Qdots to form the final Pdot−Qdot hybrid.

Figure 1A outlines our strategy in more detail. We synthesized PFBT with amino functional groups, allowing us to convert these amino groups to thiols using 2-iminothiolane (Traut's reagent) in tetrahydrofuran (THF) in an effort to have an efficient ligand exchange process with the original amino capping ligands on the Qdot surface. After the ligand exchange reaction, we blended PFBT with a polystyrene−poly(ethylene glycol)−COOH (PS−PEG−COOH) copolymer containing the carboxyl groups needed for further bioconjugation of Pdots. The polymer−Qdot solution was coprecipitated in water under sonication to form the final Pdot−Qdot NPs. It is worth mentioning that when 2-iminothiolane was not added during the ligand exchange process, the resulting Pdot−Qdot NPs aggregated within 12 h, demonstrating the importance of the conversion of the amines to thiols in order to have efficient ligand exchange between the polymers and the original amino capping ligands on the Qdot surface. From transmission electron microscopy (TEM) images (Figure 1B), we can clearly see that clusters of Qdots were encapsulated in the Pdots, with ~30 Qdots embedded inside each individual hybrid NP. Dynamic light scattering (DLS) measurements also showed that the average diameter of the Pdot−Qdot NPs was ~25 nm (Figure 1C).

It is worth mentioning that the crystalline structure of the Qdots remained intact during the preparation processes (Figure 1B), which is important in preserving the optical properties of the Qdots. Furthermore, this Pdot−Qdot hybrid remained optically stable and biologically active for at least 2 months of
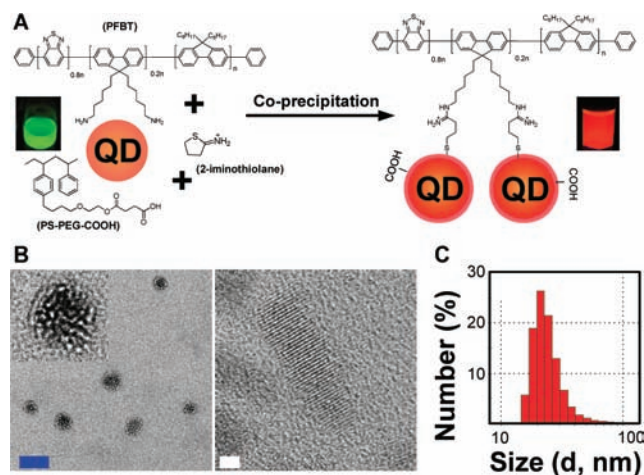
Figure 1. (A) Schematic showing the preparation of Pdot–Qdot hydrid NPs. The terminal amino groups of the amine-functionalized PFBT were first converted to thiols to enable covalent binding of PFBT to the surfaces of Qdots (labeled as QD), after which the Pdot–Qdot solution was mixed with PS–PEG–COOH in THF and then co-condensed in water via nanoprecipitation under vigorous sonication to form Qdot-embedded Pdots. (B) TEM images of Pdot–Qdot NPs. The inset in the upper-left corner shows an enlarged view of a single Pdot–Qdot NP. The blue and white scale bars represent 20 and 2 nm, respectively. (C) Histogram of hydrodynamic diameters of Pdot–Qdot NPs measured by DLS. The average diameter was ∼25 nm.

storage at 4 °C in physiological pH buffers (see below). We noticed that the color of emission changed drastically from bright-yellow fluorescence before nanoprecipitation to deep-red emission after nanoprecipitation. Because the yellow fluorescence is characteristic of PFBT while the red fluorescence is from the Qdots, this phenomenon is indicative of highly efficient energy transfer from PFBT to the Qdots, which were in close contact after nanoprecipitation and formation of the Pdot–Qdot hybrid.

Figure 2A shows a typical absorption spectrum of Pdot–Qdot NPs. The absorption peak at ∼450 nm (blue arrow) is from PFBT, and the weak absorption at ∼640 nm (red arrow) is from CdSe Qdots; the strong absorption below 400 nm is attributed to both PFBT and Qdots. In the present work, we employed three different sizes of Qdots that emit at 655 nm (QD655), 705 nm (QD705), and 800 nm (QD800). These were commercially available from Invitrogen. We carefully optimized the PFBT/Qdot ratio [see the Supporting Information (SI)] in order to have efficient energy transfer from PFBT to the Qdots while aiming to have a compact size (i.e., a minimal number of Qdots inside a Pdot). Therefore, different numbers of Qdots were encapsulated inside the Pdots for the different sizes of Qdots that we employed. As shown in Figure 2B, the fluorescence emission of PFBT (black arrow) was almost completely quenched, indicating efficient energy/electron transfer from PFBT to the Qdots. We also measured the time-resolved fluorescence decay curves of QD655 and the Pdot–QD655 hybrid (Figure S5 in the SI) to provide further confirmation of the energy transfer between PFBT and the Qdots.

More importantly, the emission bandwidth of the Pdot–Qdot NPs remained unaltered in comparison with the original Qdot emission, thereby allowing us to create Pdot-based NPs that retain the narrow emission characteristics of Qdots. In the case of QD655, for example, the full width at half-maximum of
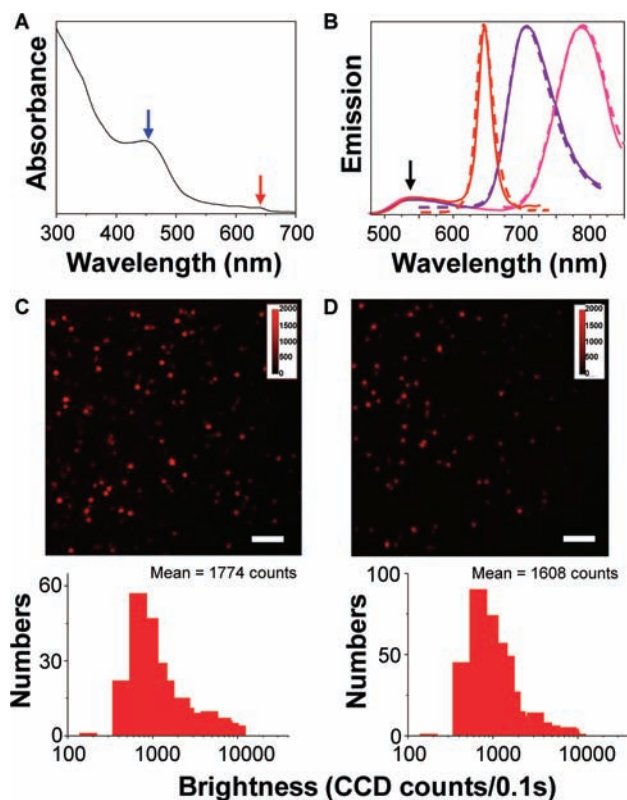

Figure 2. Characterization of Pdot–Qdot NPs. (A) UV–vis spectrum of Pdot–Qdot NPs in water. (B) Emission spectra of QD655 (dashed red line), QD705 (dashed purple line), and QD800 (dashed pink line) in decane. Emission spectra of their corresponding Pdot–Qdot forms after nanoprecipitation are shown as solid lines. (C) Single-particle fluorescence images of PFBT–DBT Pdots (upper panel) and the corresponding histograms showing the intensity distributions (bottom panel). (D) Single-particle fluorescence images of PFBT–QD655 Pdot–Qdot NPs (upper panel) and the corresponding histograms showing the intensity distributions (bottom panel). The scale bars are 4 μm. Each histogram is based on measurements of at least 700 individual particles.

the emission band of Pdot–QD655 NPs in water was ∼25 nm (solid red line in Figure 2B), which was essentially the same as the width of the original QD655 emission in decane (dashed red line). We also demonstrated that this technique can be applied to NIR-emitting Qdots such as QD705 and QD800 (purple and pink lines in Figure 2B).

The quantum yields of the Pdot–QD655, Pdot–QD705, and Pdot–QD800 NPs in buffer solutions were determined to be 23, 38, and 29%, respectively, while the quantum yields of QD655, QD705, and QD800 after they were transferred from decane to aqueous solution were 27, 41, and 32%, respectively. This implies that we should be able to take advantage of the unique optical properties of Qdots, such as narrow-band NIR emission, without sacrificing their high quantum yields, while also implanting on them the merits of Pdots, including the large absorption cross sections and facile surface functionalization offered by Pdots.

To understand the performance of the Pdot–Qdot NPs, we measured their single-particle fluorescence brightness (Figure 2C,D). In our previous work, we established that for Pdots consisting of PFBT blended with 4,7-di-2-thienyl-2,1,3-benzothiadiazole (DBT), each single PFBT–DBT Pdot emitting at ∼650 nm is ∼15 times brighter than a single

QD655.[25] Therefore, here we directly compared the single-particle brightnesses of PFBT–DBT Pdots and PFBT–QD655 NPs and found them to be similar (Figure 2C,D), which suggests that the particle brightness of the PFBT–QD655 NPs is in turn ~15 times brighter than that of a single QD655. Because the particle brightness is given by the product of the absorption cross section and quantum yield and because the quantum yields of QD655 and Pdot–QD655 NPs are comparable, we can ascribe most of the brightness enhancement to the vast increase in the optical absorption cross section provided by the semiconducting polymer coating or/and Qdot multiples.

We next employed Pdot–Qdot NPs for both cell-surface and subcellular labeling to demonstrate their potential in biological applications. In one experiment, we performed subcellular microtubule labeling in HeLa cells. Here we first conjugated streptavidin onto the surface of Pdot–Qdot NPs via 1-ethyl-3-[3-dimethylaminopropyl]carbodiimide hydrochloride (EDC)-catalyzed coupling (see the SI). We then incubated the Pdot–Qdot–streptavidin hybrid together with biotinylated monoclonal anti-α-tubulin antibody with HeLa cells so the Pdot–Qdot–streptavidin NPs could label the microtubules of HeLa cells. Figure 3A–C shows representative confocal images of Pdot–QD705–streptavidin-labeled microtubules in HeLa cells, indicating that the Pdot–Qdot–streptavidin NPs could be specifically targeted onto subcellular structures in the presence of biotinylated antibody. However, because of the relatively large particle size of the Pdot–Qdot NPs, the tail regions of the microtubules could not be well resolved (Figure 3A). To obtain particles with smaller sizes, if needed, further experimentation of suitable polymer–Qdot pairs is required. No noticeable fluorescence signal from Pdot–Qdot NPs was observed for negative control samples (Figure 3D–F) where the experimental conditions were identical to those in Figure 3A–C except for the absence of the biotinylated primary antibody. These results indicate that this new class of fluorescent hybrid probes exhibits highly specific binding activity with minimal nonspecific absorption.

Additionally, we also carried out flow cytometry experiments in which Pdot–QD705 and Pdot–QD800 NPs were used to label membrane proteins on MCF-7 cells. Here the Pdot–Qdot–streptavidin conjugates, together with primary biotin anti-human CD326 EpCAM antibody and biotinylated goat anti-mouse IgG secondary antibody, were labeled onto the surfaces of live MCF-7 cells. Pdot–QD705 and Pdot–QD800 NPs have emissions in the NIR, which is beneficial in many biological studies. Figure 3G,H shows the flow cytometry results for Pdot–QD705 and Pdot–QD800 NPs, respectively. Both probes showed excellent separation between Pdot–Qdot–streptavidin-labeled cells (purple/pink line, with primary antibody) and the negative control/background (black lines, without primary antibody). These results demonstrate that Pdot–Qdot bioconjugates can be targeted to MCF-7 cells effectively and specifically with ultralow nonspecific binding, consistent with the results from confocal microscopy in HeLa cells.

For practical applications and translation of the Pdot–Qdot hybrid for widespread adoption, the colloidal stability and storability of the Pdot–Qdot solution is important. To assess this aspect, we stored the Qdot-embedded Pdots at 4 °C for 2 months in a buffer solution. We then used flow cytometry to evaluate the fluorescence of the labeled cells as well as the negative control, which would be affected by the presence of
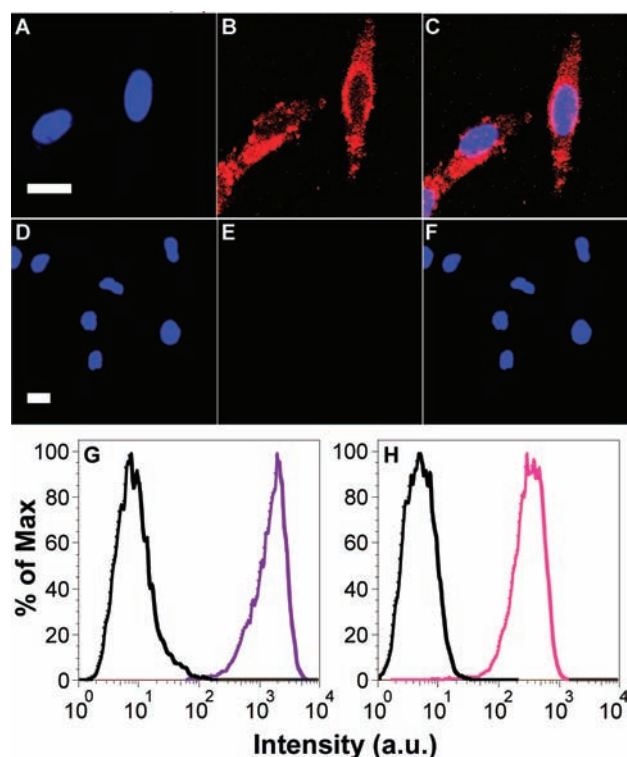

Figure 3. (A–F) Two-color confocal microscopy images of microtubules in HeLa cells labeled with Pdot–QD705–streptavidin NPs. The blue fluorescence is from the nuclear counterstain Hoechst 34580, and the red fluorescence is from Pdot–QD705–streptavidin NPs. (A) Image of nuclei. (B) Image of microtubules. (C) Overlay of panels (A) and (B). (D–F) Images of negative control samples where cells were incubated with Pdot–QD705–streptavidin NPs in the absence of the biotinylated primary antibody. The scale bars are 20 μm. (G, H) Flow cytometry detection of Pdot–Qdot-labeled MCF-7 cells. The purple and pink lines show the fluorescence intensity distributions of Pdot–QD705–streptavidin- and Pdot–QD800–streptavidin-labeled cells, respectively. The black lines represent the results for negative control samples where no primary biotin anti-human CD326 EpCAM antibody was present.

any nonspecific absorption. As shown in Figure S2, in the case of Pdot–QD800–streptavidin NPs as an example, we observed a negligible change in the fluorescence of labeled MCF-7 cells and no increase in nonspecific binding, which indicates excellent colloidal stability and storability. Furthermore, no particle aggregation or size increase was found from DLS measurements after 2 months of storage (data not shown).

In summary, we have developed a new class of nanocomposites made of Pdots and Qdots that exhibit combined functionalities and optical properties that are superior to those of either type of nanoparticle. The hybrid nanoparticles possess high brightness with narrow NIR emission, easy optical tunability, and facile surface chemistry, which are not available simply from Pdots or Qdots alone. We envision that this new nanocomposite can be utilized for a variety of biological applications, including specific in vitro and in vivo cellular imaging. In addition to bioimaging by integration with our recent advances in sensing physiologically important species using Pdots,[21,22,26] these hybrid nanomaterials should also afford a new means of biological or environmental analysis.

ASSOCIATED CONTENT

ⓢ Supporting Information

Synthesis of PFBT with amino functional groups, Pdot−Qdot preparation and characterization, experimental section, cell culturing and labeling, and Figures S1−S5. This material is available free of charge via the Internet at http://pubs.acs.org.

AUTHOR INFORMATION

Corresponding Author

chiu@chem.washington.edu

Notes

The authors declare no competing financial interest.

ACKNOWLEDGMENTS

REFERENCES

(1) Jin, Y.; Gao, X. *Nat. Nanotechnol.* **2009**, *4*, 571−576.

(2) Hu, S.-H.; Gao, X. *J. Am. Chem. Soc.* **2010**, *132*, 7234−7237.

(3) Zhang, J.; Tang, Y.; Lee, K.; Ouyang, M. *Science* **2010**, *327*, 1634−1638.

(4) Jones, M. R.; Osberg, K. D.; Macfarlane, R. J.; Langille, M. R.; Mirkin, C. A. *Chem. Rev.* **2011**, *111*, 3736−3827.

(5) Donegá, C. d. M. *Chem. Soc. Rev.* **2011**, *40*, 1512−1546.

(6) Behrens, S. *Nanoscale* **2011**, *3*, 877−892.

(7) Buck, M. R.; Bondi, J. F.; Schaak, R. E. *Nat. Chem.* **2012**, *4*, 37−44.

(8) Medintz, I. L.; Uyeda, H. T.; Goldman, E. R.; Mattoussi, H. *Nat. Mater.* **2005**, *4*, 435−446.

(9) Somers, R. C.; Bawendi, M. G.; Nocera, D. G. *Chem. Soc. Rev.* **2007**, *36*, 579−591.

(10) Choi, H. S.; Liu, W.; Misra, P.; Tanaka, E.; Zimmer, J. P.; Ipe, B. I.; Bawendi, M. G.; Frangioni, J. V. *Nat. Biotechnol.* **2007**, *25*, 1165−1170.

(11) Michalet, X.; Pinaud, F. F.; Bentolila, L. A.; Tsay, J. M.; Doose, S.; Li, J. J.; Sundaresan, G.; Wu, A. M.; Gambhir, S. S.; Weiss, S. *Science* **2005**, *307*, 538−544.

(12) Derfus, A. M.; Chan, W. C. W.; Bhatia, S. N. *Nano Lett.* **2004**, *4*, 11−18.

(13) Wu, C.; Bull, B.; Szymanski, C.; Christensen, K.; McNeill, J. *ACS Nano* **2008**, *2*, 2415−2423.

(14) Howes, P.; Green, M.; Levitt, J.; Suhling, K.; Hughes, M. *J. Am. Chem. Soc.* **2010**, *132*, 3989−3996.

(15) Kaeser, A.; Schenning, A. P. H. J. *Adv. Mater.* **2010**, *22*, 2985−2997.

(16) Pecher, J.; Mecking, S. *Chem. Rev.* **2010**, *110*, 6260−6279.

(17) Tian, Z.; Yu, J.; Wu, C.; Szymanski, C.; McNeill, J. *Nanoscale* **2010**, *2*, 1999−2011.

(18) Tuncel, D.; Demir, H. V. *Nanoscale* **2010**, *2*, 484−494.

(19) Wu, C.; Jin, Y.; Schneider, T.; Burnham, D. R.; Smith, P. B.; Chiu, D. T. *Angew. Chem., Int. Ed.* **2010**, *49*, 9436−9440.

(20) Wu, C.; Schneider, T.; Zeigler, M.; Yu, J.; Schiro, P. G.; Burnham, D. R.; McNeill, J. D.; Chiu, D. T. *J. Am. Chem. Soc.* **2010**, *132*, 15410−15417.

(21) Chan, Y.-H.; Jin, Y.; Wu, C.; Chiu, D. T. *Chem. Commun.* **2011**, *47*, 2820−2822.

(22) Chan, Y.-H.; Wu, C.; Ye, F.; Jin, Y.; Smith, P. B.; Chiu, D. T. *Anal. Chem.* **2011**, *83*, 1448−1455.

(23) Jin, Y.; Ye, F.; Zeigler, M.; Wu, C.; Chiu, D. T. *ACS Nano* **2011**, *5*, 1468−1475.

(24) Petkau, K.; Kaeser, A.; Fischer, I.; Brunsveld, L.; Schenning, A. P. H. J. *J. Am. Chem. Soc.* **2011**, *133*, 17063−17071.

(25) Wu, C.; Hansen, S. J.; Hou, Q.; Yu, J.; Zeigler, M.; Jin, Y.; Burnham, D. R.; McNeill, J. D.; Olson, J. M.; Chiu, D. T. *Angew. Chem., Int. Ed.* **2011**, *50*, 3430−3434.

(26) Ye, F.; Wu, C.; Jin, Y.; Chan, Y.-H.; Zhang, X.; Chiu, D. T. *J. Am. Chem. Soc.* **2011**, *133*, 8146−8149.

(27) Jin, Y.; Ye, F.; Wu, C.; Chan, Y.-H.; Chiu, D. T. *Chem. Commun.* **2012**, *48*, 3161−3163.

(28) Ye, F.; Wu, C.; Jin, Y.; Wang, M.; Chan, Y.-H.; Yu, J.; Sun, W.; Hayden, S.; Chiu, D. T. *Chem. Commun.* **2012**, *48*, 1778−1780.